SUPPORTING INFORMATION

Dirac half-semimetallicity and antiferromagnetism in graphene nanoribbon/hexagonal boron nitride heterojunctions

Nikita V. Tepliakov,[*,†,‡] Ruize Ma,[†,‡,¶] Johannes Lischner,[†,‡] Efthimios Kaxiras,[§,‖] Arash A. Mostofi,[†,‡] and Michele Pizzochero[*,‖]

†*Departments of Materials and Physics, Imperial College London, London SW7 2AZ, United Kingdom*

‡*The Thomas Young Centre for Theory and Simulation of Materials, Imperial College London, London SW7 2AZ, United Kingdom*

¶*Department of Physics, University of Oxford, Oxford OX1 2JD, United Kingdom*

§*Department of Physics, Harvard University, Cambridge, MA 02138, United States*

‖*School of Engineering and Applied Sciences, Harvard University, Cambridge, MA 02138, United States*

E-mail: n.tepliakov20@imperial.ac.uk; mpizzochero@g.harvard.edu

Contents

Supporting Note S1: Details of *ab initio* calculations S3

Supporting Note S2: Exchange-correlation density functionals S4

Supporting Note S3: Lattice strain in ZGNR/hBN heterojunctions S5

Supporting Note S4: Structural disorder in ZGNR/hBN heterojunctions S6

Supporting Note S5: Density of states of ZGNR/hBN heterojunctions S7

Supporting Note S6: Crystallographic orientation of ZGNR/hBN heterojunctions S8

Supporting Note S7: Band structure of armchair GNR/hBN heterojunctions . S9

Supporting Note S8: Details of mean-field Hubbard model calculations S10

Supporting Note S9: U/t parameters of the mean-field Hubbard model S11

Supporting Note S10: Hopping parameters in the mean-field Hubbard model . S12

Supporting Note S11: Phase diagram from mean-field Hubbard model S13

Supporting Note S12: Edge effects in ZGNR/hBN heterojunctions S14

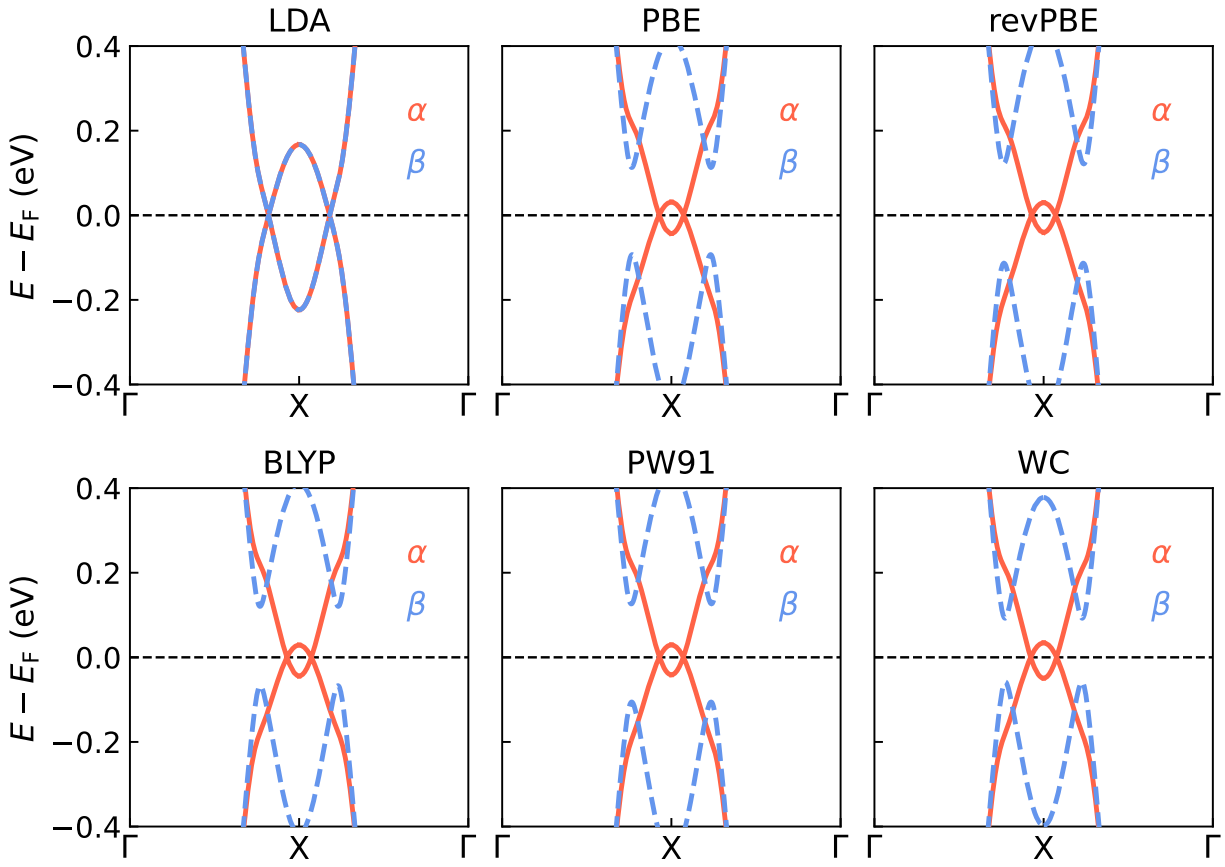
Supporting Note S13: Charge doping in hydrogen-terminated ZGNRs S15

Supporting References **S16**

Supporting Note S1: Details of *ab initio* calculations

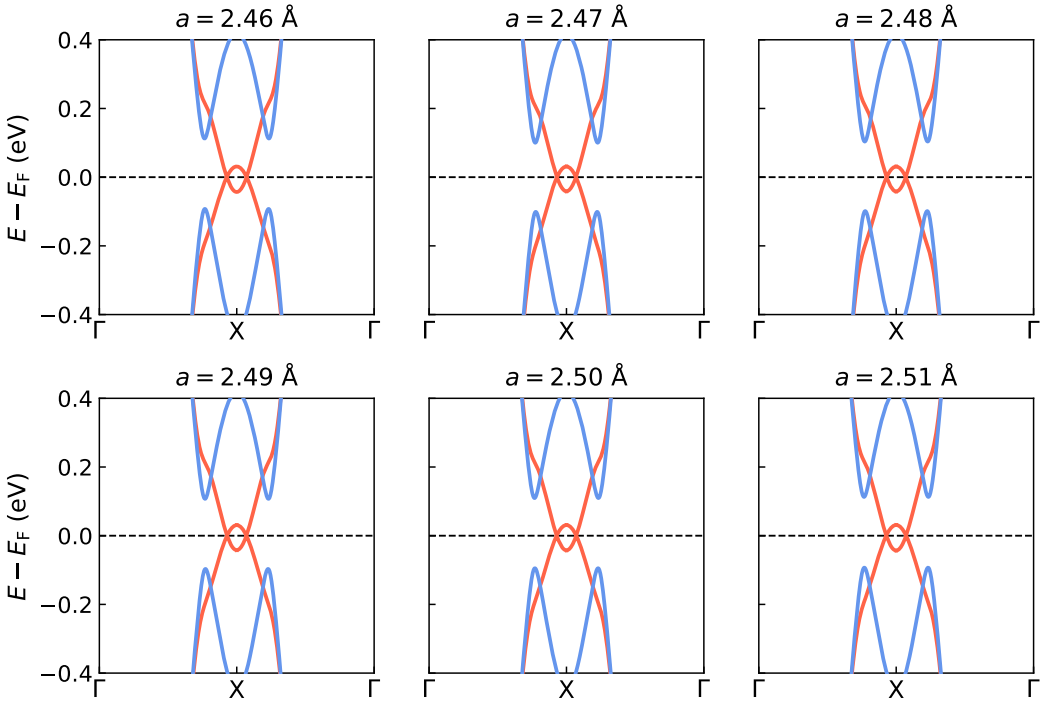
Our *ab initio* calculations are based on density-functional theory,[S1] as implemented in the SIESTA package.[S2] We adopt the gradient-corrected approximation to the exchange-correlation functional proposed by Perdew, Burke, and Ernzerhof,[S3] but have explicitly verified that our results are robust with respect to the choice of the functional, with the exception of the simplest local-density approximation; see Supporting Note S2. The Kohn-Sham valence orbitals are expanded in a linear combination of atom-centered basis functions at the single-ζ plus single polarization level. Atomic nuclei and core electrons are represented by norm-conserving pseudopotentials generated according to the Troullier-Martins scheme.[S4] We use a mesh cutoff of 300 Ry for all calculations except for the Bader charge analysis,[S5] for which this value is increased to 500 Ry. The lattice constant of ZGNR/hBN heterojunctions is constrained to that of hexagonal boron nitride, 2.51 Å. Throughout our work, our models consist of orthorhombic supercells of size $a = 86.92$ Å, $b = 2.51$ Å, and $c = 20.00$ Å for the ZGNR/hBN heterojunctions and $a = 86.92$ Å, $b = 2.46$ Å, and $c = 20.00$ Å for hydrogen-terminated ZGNRs. The integration over the Brillouin zone is carried out using a grid of $1 \times 15 \times 1$ k-points for all calculations but the density of states, for which the grid is increased by a factor of eighty in each periodic direction. The atomic structure is relaxed at charge neutrality until the maximum force component on each atom is lower in magnitude than 0.02 eV/Å. The structural models of ZGNR/hBN heterojunctions adopted in our *ab initio* calculations ensure a large lateral distance between periodic replicas. For example, in the case of a ZGNR of width $w = 1.4$ nm (i.e., the representative width discussed in the main text) embedded in hBN, such distance is 73 Å. Because of the large spatial separation between adjacent nanoribbons, each ZGNR can be considered isolated in the hBN sheet. Hence, our models closely resemble the experimental situation where graphene nanoribbons are grown in two-dimensional hexagonal boron nitride.[S6,S7] Our approach differ from previous works, where ZGNR/hBN heterojunctions were described as, e.g., periodically repeated, alternated strips of hBN and ZGNR[S8–S10] or a single interface in a hybrid hBN/ZGNR nanoribbon.[S11]

Supporting Note S2: Exchange-correlation density functionals



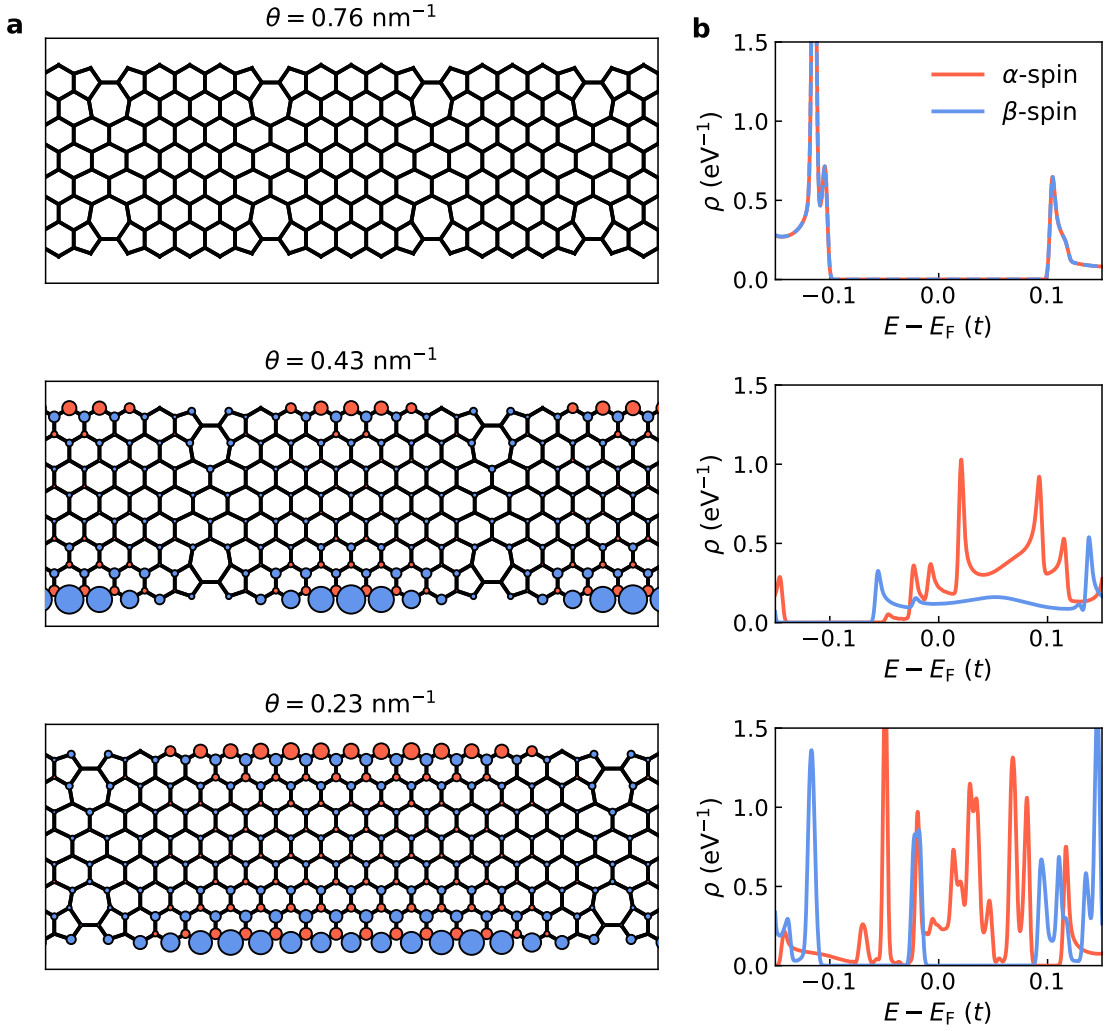
Band structure of a zigzag graphene nanoribbon of width $w = 1.4$ nm embedded in hexagonal boron nitride, as obtained at the density-functional theory level for different exchange-correlation functionals, i.e., LDA,[S12,S13] PBE,[S3] revPBE,[S14] BLYP,[S15–S17] PW91,[S18] and WC.[S19] Red and blue lines denote α- and β-spin contributions, respectively. Energies are referenced to the Fermi level (E_F).

Supporting Note S3: Lattice strain in ZGNR/hBN heterojunctions



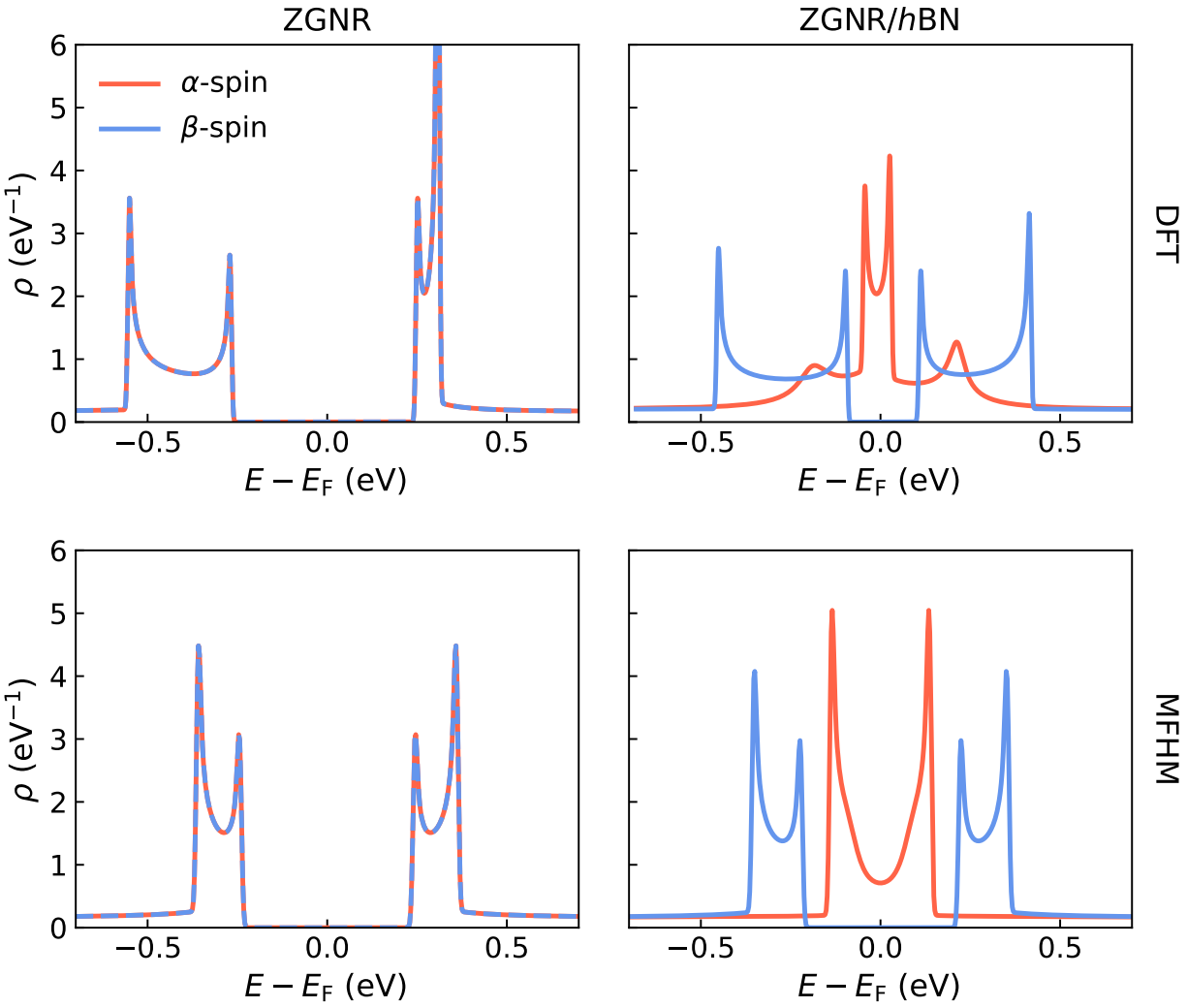
Electronic band structure of a zigzag graphene nanoribbon of width $w = 1.4$ nm embedded into hexagonal boron nitride of different for different values of lattice constant (a). Red and blue lines denote α- and β-spin contributions, respectively. Energies are referenced to the Fermi level (E_F). The half-semimetallic phase is found to be robust with respect to the application of a moderate lattice strain.

Supporting Note S4: Structural disorder in ZGNR/hBN heterojunctions



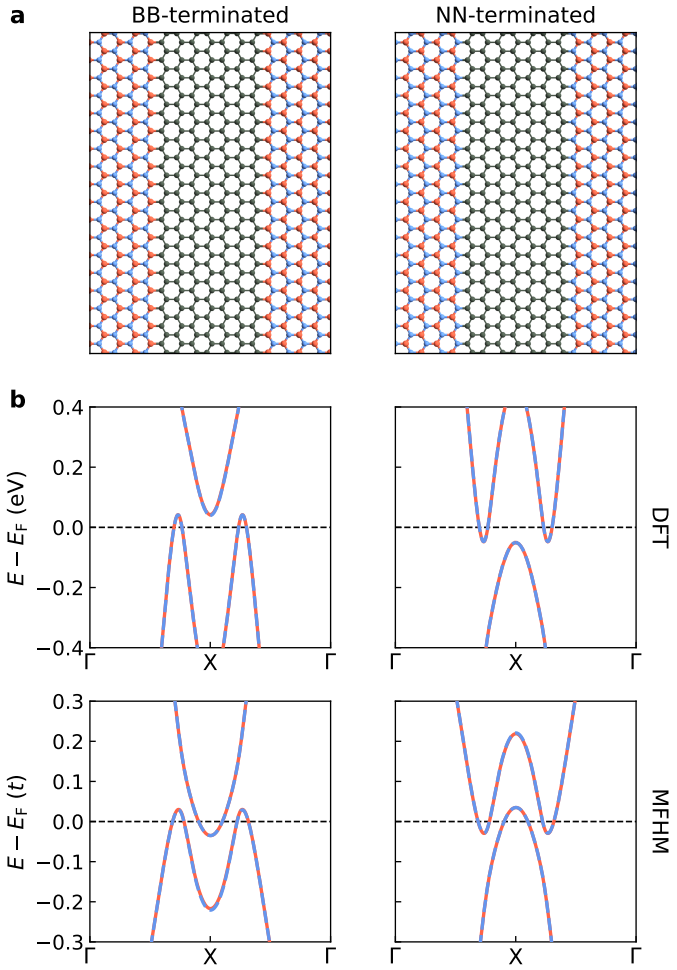
(a) Atomic structure of ZGNRs of width $w = 1.6$ nm hosting a pair of dislocation-type defects[S20] of increasing density θ; also superimposed is the spin density, as obtained from the mean-field Hubbard model (MFHM) calculations, where red and blue circles indicate magnetization of opposite orientation. (b) Corresponding spin-resolved density of states. Red and blue lines denote α- and β-spin contributions, respectively. Energies are referenced to the Fermi level (E_F). To emulate the effect of hBN surrounding the ZGNR in the ZGNR/hBN heterojunction, the edge potentials in the MFHM are set to $\epsilon_1 = 0.45t$ and $\epsilon_2 = -0.45t$. Depending on the density of defects θ, a non-magnetic semiconducting ($\theta = 0.76$ nm^{-1}), ferrimagnetic metallic ($\theta = 0.43$ nm^{-1}), or ferrimagnetic half-metallic ($\theta = 0.23$ nm^{-1}) phase emerges in the ZGNR/hBN heterojunction.

Supporting Note S5: Density of states of ZGNR/hBN heterojunctions



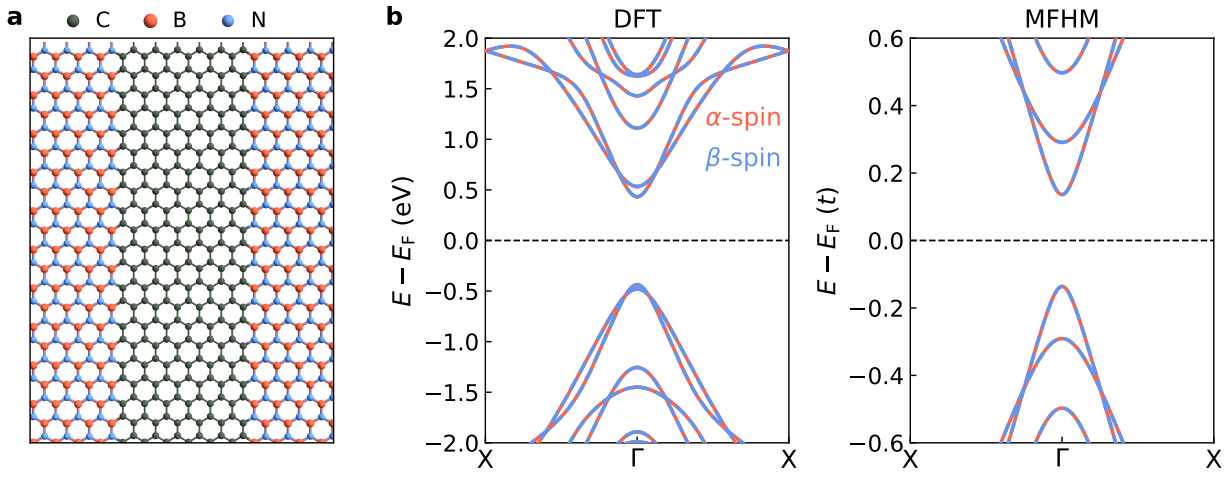
Total electronic density of states (ρ) of hydrogen-terminated ZGNR (left panels) and ZGNR/hBN heterojunction (right panels) of width $w = 1.4$ nm, as obtained from density-functional theory (top panels) and mean-field Hubbard model (bottom panels). The value of electron-electron repulsion in the MFHM is set to $U = t$, where t is the nearest-neighbor hopping integral, and the potentials on the edges of the ZGNR embedded in hBN are $\epsilon_1 = -\epsilon_2 = 0.2t$. Red and blue lines denote α- and β-spin contributions, respectively. Energies are referenced to the Fermi level (E_F).

Supporting Note S6: Crystallographic orientation of ZGNR/hBN heterojunctions



(a) Atomic structure of a zigzag graphene nanoribbon (ZGNR) of width $w = 1.4$ nm connected to two sheets of hexagonal boron nitride of different orientation. Left and right panels show the two different cases in which the edges of the ZGNR are both terminated with either B or N atoms. Red, blue, and black spheres denote boron, nitrogen, and carbon atoms, respectively. (b) Electronic band structure of the B- and N-terminated ZGNR, calculated using density-functional theory (DFT) and mean-field Hubbard model (MFHM). In DFT calculations, hydrogen-terminated finite-size models have been adopted. In the MFHM calculations, the value of electron-electron repulsion in the MFHM is set to $U = t$, where t is the nearest-neighbor hopping integral; the edge potentials for B-terminated ZGNRs are set to $\epsilon_1 = 0.45t$ and $\epsilon_2 = 0.45t$, whereas N-terminated ZGNRs have $\epsilon_1 = -0.45t$ and $\epsilon_2 = -0.45t$. Red and blue lines denote α- and β-spin contributions, respectively. Energies are referenced to the Fermi level (E_F).

Supporting Note S7: Band structure of armchair GNR/hBN heterojunctions

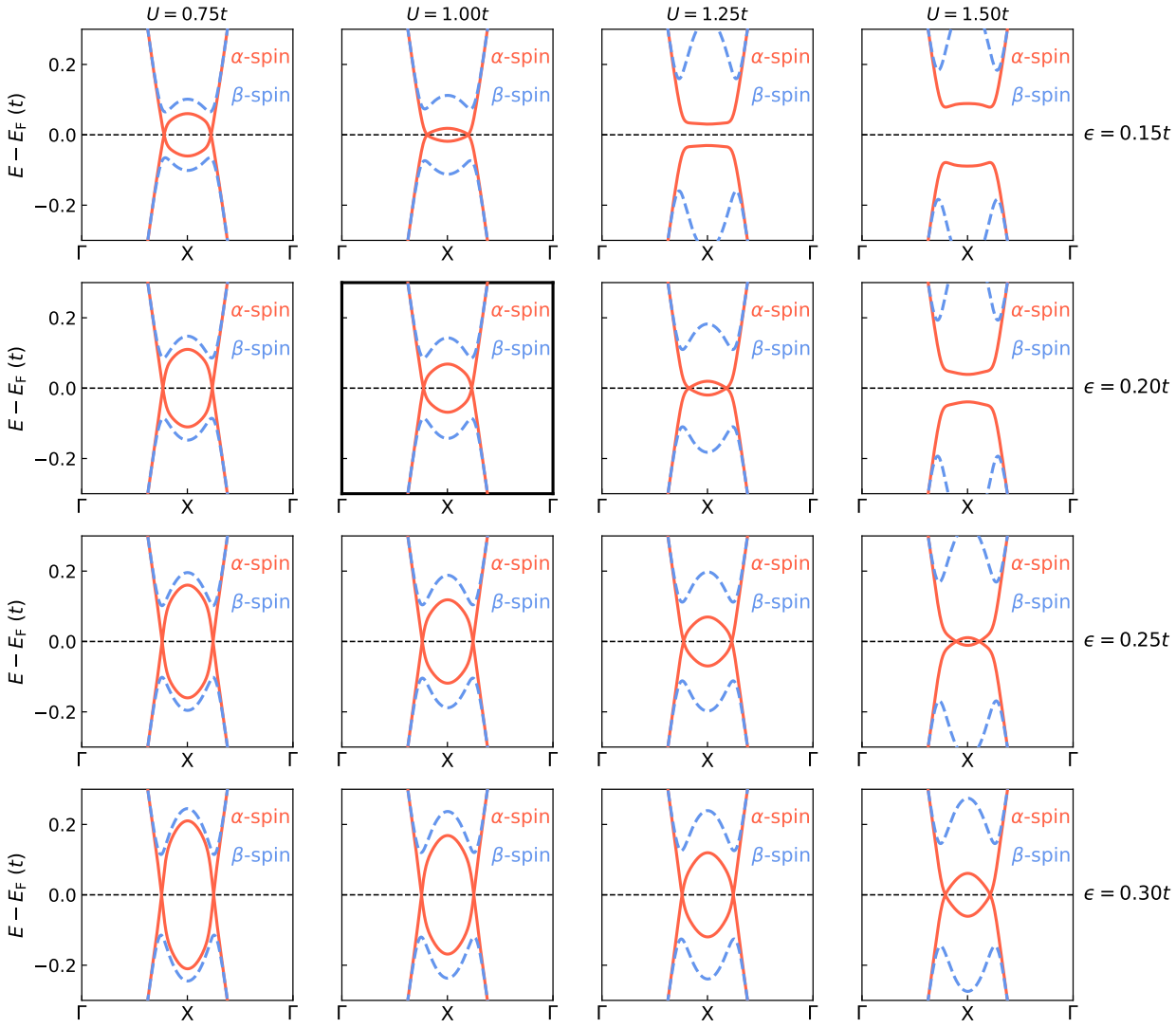


(a) Atomic structure of an armchair graphene nanoribbon (AGNR) of width $w = 1.4$ nm embedded in hexagonal boron nitride. Red, blue, and black spheres denote boron, nitrogen, and carbon atoms, respectively. (b) Electronic band structure of the AGNR embdedded in hBN, calculated using density-functional theory (DFT) and mean-field Hubbard model (MFHM). In the MFHM calculations, the value of electron-electron repulsion in the MFHM is set to $U = t$, where t is the nearest-neighbor hopping integral; the potentials on carbon atoms terminated by B atoms are set to $\epsilon = 0.2t$, whereas the potentials on N-terminated carbon atoms are set to $\epsilon = -0.2t$. Red and blue lines denote α- and β-spin contributions, respectively. Energies are referenced to the Fermi level (E_{F}).

Supporting Note S8: Details of mean-field Hubbard model calculations

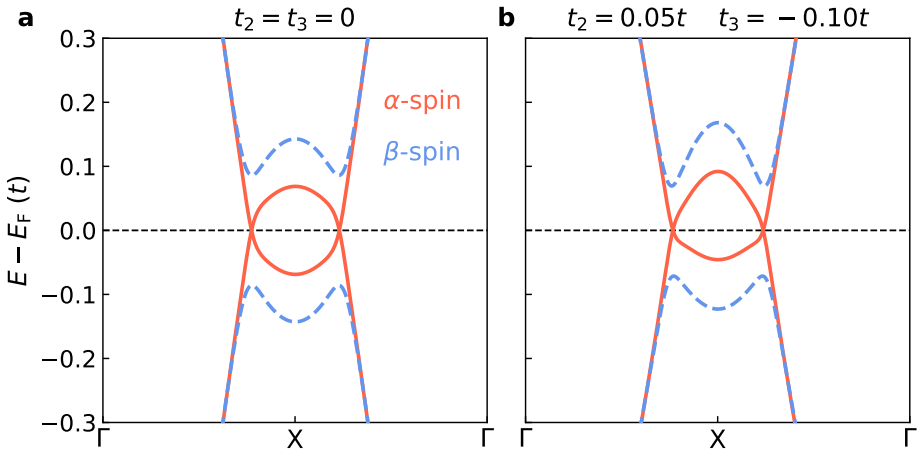
The mean-field Hubbard Hamiltonian given in Eq. (1) in the main text is solved self-consistently. To that end, we begin by considering $\epsilon_i = 0$ and initializing the electron density $\langle \hat{n}_{i,\sigma} \rangle$ such that the spins residing at the different edges of the nanoribbon have an antiparallel orientation. We solve the Hamiltonian iteratively to obtain the converged electron densities $\langle \hat{n}_{i,\sigma} \rangle$. Next, we introduce the on-site potentials ϵ_i as a first-order perturbation to the energies of electronic states. This is possible even when the energy bands cross at the Fermi level due to the localization of the corresponding states at the opposite edges of the nanoribbon, which results in vanishing matrix elements coupling these bands. Finally, we re-calculate the electron densities $\langle \hat{n}_{i,\sigma} \rangle$, which may have changed due to the crossing of energy bands at the Fermi level, and perform a final diagonalization of the model Hamiltonian. Although we set $U/t = 1$, as detailed in the main text, we have additionally investigated the interplay between the model parameters U/t and ϵ; see Supporting Note S5.

Supporting Note S9: U/t parameters of the mean-field Hubbard model



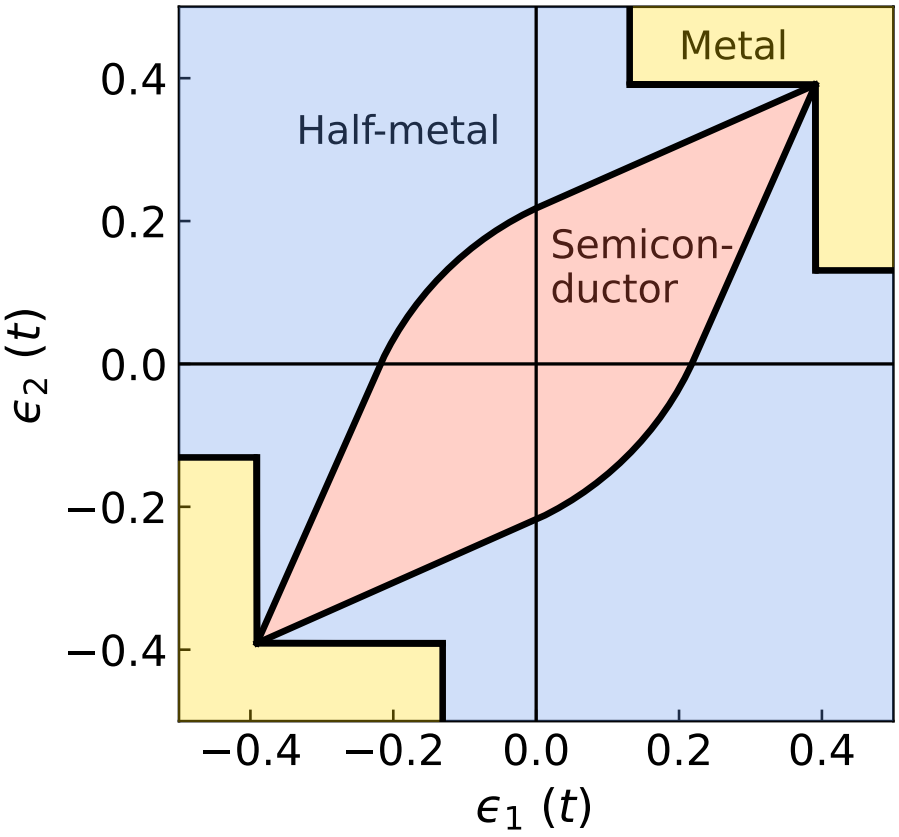
Band structure of a zigzag graphene nanoribbon of width $w = 1.4$ nm embedded in hexagonal boron nitride, as obtained using the mean-field Hubbard model Hamiltonian described in the main text, for increasing values of electron-electron repulsion U and potentials on the two edges set to $\epsilon_1 = -\epsilon_2 = \epsilon$. All parameters are expressed in units of the nearest-neighbor hopping integral t. The highlighted case with $U = t$ and $\epsilon = 0.2t$ corresponds to the choice of parameters adopted in the main text. Red and blue colors denote α- and β-spin contributions, respectively. Energies are referenced to the Fermi level (E_{F}).

Supporting Note S10: Hopping parameters in the mean-field Hubbard model



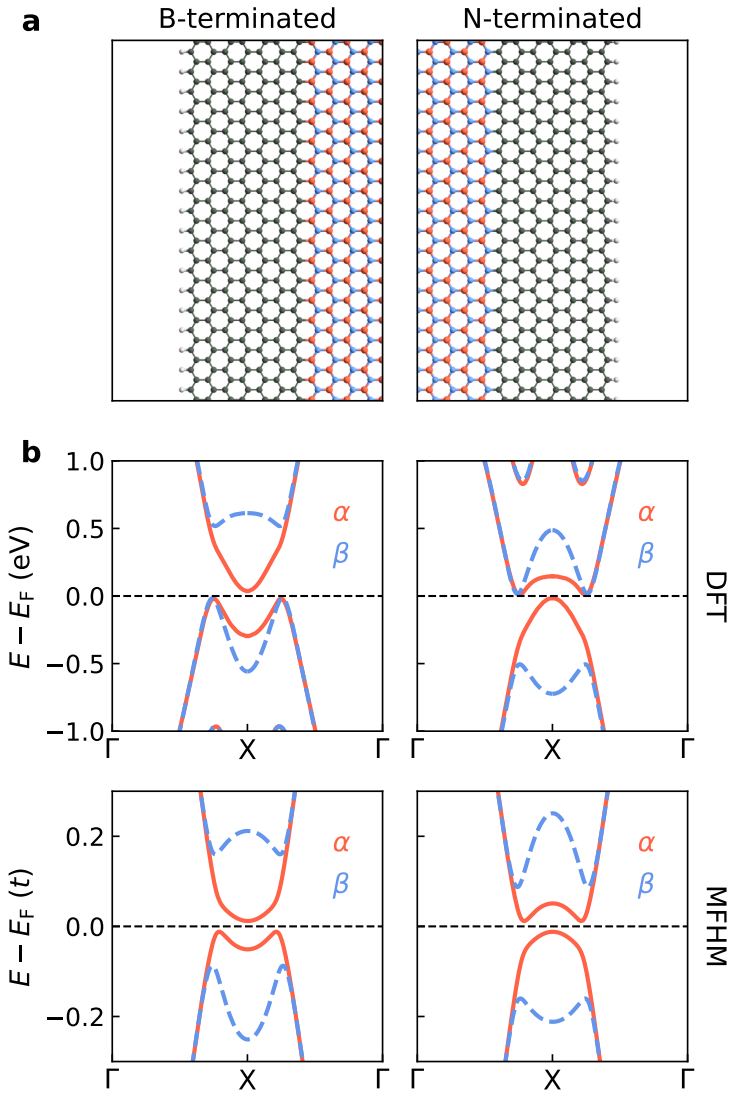
Band structure of a zigzag graphene nanoribbon of width $w = 1.4$ nm embedded in hexagonal boron nitride, as obtained using the mean-field Hubbard model Hamiltonian, either (a) accounting only for the nearest-neighbor hopping interaction $-t$ or (b) including second and third nearest-neighbor hopping interactions $t_2 = 0.05t$ and $t_3 = -0.10t$. Such hopping parameters have been previously derived from Wannierization of *ab initio* electronic structure.[S21] The value of electron-electron repulsion is set to $U = t$ and the potentials on the two edges are set to $\epsilon_1 = -\epsilon_2 = 0.2t$. All parameters are expressed using the absolute value of the first nearest-neighbor hopping integral t. Red and blue colors denote α- and β-spin contributions, respectively. Energies are referenced to the Fermi level (E_F). The half-semimetallic phase is found to be robust against long-range hopping interactions.

Supporting Note S11: Phase diagram from mean-field Hubbard model



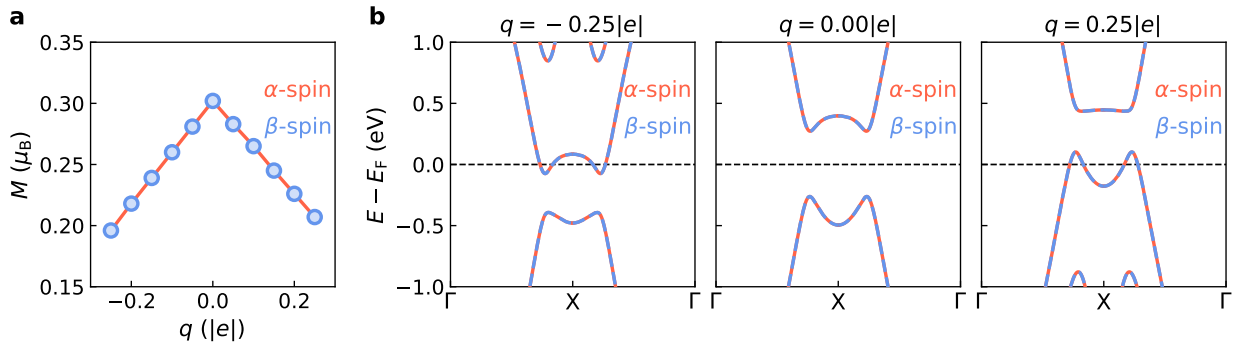
Global electronic phase diagram of ZGNR of width $w = 1.4$ nm as a function of on-site potentials (ϵ_1 and ϵ_2) on the edges, as obtained from the mean-field Hubbard model Hamiltonian. Red, blue, and yellow shaded areas indicate semiconducting, half-metallic, and metallic phases, respectively. Note that Figure 3(b) in the main text corresponds to the bottom right quadrant of this extended phase diagram.

Supporting Note S12: Edge effects in ZGNR/hBN heterojunctions



(a) Atomic structure of a zigzag graphene nanoribbon (ZGNR) of width $w = 1.4$ nm connected to hexagonal boron nitride on one edge and terminated with hydrogen atoms on the other edge.[S11] Left and right panels show two different cases in which the edge of the ZGNR is terminated with either B or N atoms. Red, blue, black, and white spheres denote boron, nitrogen, carbon, and hydrogen atoms, respectively. (b) Electronic band structure of the B- and N-terminated ZGNR, calculated using density-functional theory (DFT) and mean-field Hubbard model (MFHM). The value of electron-electron repulsion in the MFHM is set to $U = t$, where t is the nearest-neighbor hopping integral; the edge potentials for B-terminated ZGNRs are set to $\epsilon_1 = 0.2t$ and $\epsilon_2 = 0$, whereas N-terminated ZGNRs have $\epsilon_1 = 0$ and $\epsilon_2 = -0.2t$. Red and blue lines denote α- and β-spin contributions, respectively. Energies are referenced to the Fermi level (E_F).

Supporting Note S13: Charge doping in hydrogen-terminated ZGNRs



(a) Magnetic moments (M) localized at the edges of a hydrogen-terminated zigzag graphene nanoribbon (ZGNR) of width $w = 1.4$ nm as a function of the excess charge (q). (b) Band structure of doped, hydrogen-terminated ZGNR for different values of q. The data is obtained using density functional theory calculations. Red and blue colors denote α- and β-spin contributions, respectively. Energies are referenced to the Fermi level (E_{F}).

Supporting References

[S1] Jones, R. O. Density functional theory: Its origins, rise to prominence, and future. *Review of Modern Physics* **2015**, *87*, 897.

[S2] Soler, J. M.; Artacho, E.; Gale, J. D.; García, A.; Junquera, J.; Ordejón, P.; Sánchez-Portal, D. The SIESTA method for *ab initio* order-N materials simulation. *Journal of Physics: Condensed Matter* **2002**, *14*, 2745.

[S3] Perdew, J. P.; Burke, K.; Ernzerhof, M. Generalized gradient approximation made simple. *Physical Review Letters* **1996**, *77*, 3865.

[S4] Troullier, N.; Martins, J. L. Efficient pseudopotentials for plane-wave calculations. *Physical Review B* **1991**, *43*, 1993.

[S5] Tang, W.; Sanville, E.; Henkelman, G. A grid-based Bader analysis algorithm without lattice bias. *Journal of Physics: Condensed Matter* **2009**, *21*, 084204.

[S6] Chen, L.; He, L.; Wang, H. S.; Wang, H.; Tang, S.; Cong, C.; Xie, H.; Li, L.; Xia, H.; Li, T.; Wu, T.; Zhang, D.; Deng, L.; Yu, T.; Xie, X.; Jiang, M. Oriented graphene nanoribbons embedded in hexagonal boron nitride trenches. *Nature Communications* **2017**, *8*, 14703.

[S7] Wang, H. S.; Chen, L.; Elibol, K.; He, L.; Wang, H.; Chen, C.; Jiang, C.; Li, C.; Wu, T.; Cong, C. X.; Pennycook, T. J.; Argentero, G.; Zhang, D.; Watanabe, K.; Taniguchi, T.; Wei, W.; Yuan, Q.; Meyer, J. C.; Xie, X. Towards chirality control of graphene nanoribbons embedded in hexagonal boron nitride. *Nature Materials* **2021**, *20*, 202.

[S8] Leon, C.; Costa, M.; Chico, L.; Latgé, A. Interface effects in hybrid hBN-graphene nanoribbons. *Scientific Reports* **2019**, *9*, 3508.

[S9] Pruneda, J. M. Origin of half-semimetallicity induced at interfaces of C-BN heterostructures. *Physical Review B* **2010**, *81*, 161409.

[S10] Ding, Y.; Wang, Y.; Ni, J. Electronic properties of graphene nanoribbons embedded in boron nitride sheets. *Applied Physics Letters* **2009**, *95*, 123105.

[S11] Liu, Y.; Wu, X.; Zhao, Y.; Zeng, X. C.; Yang, J. Half-metallicity in hybrid graphene/boron nitride nanoribbons with dihydrogenated edges. *The Journal of Physical Chemistry C* **2011**, *115*, 9442.

[S12] Ceperley, D. M.; Alder, B. J. Ground State of the Electron Gas by a Stochastic Method. *Physical Review Letters* **1980**, *45*, 566.

[S13] Perdew, J. P.; Zunger, A. Self-interaction correction to density-functional approximations for many-electron systems. *Physical Review B* **1981**, *23*, 5048.

[S14] Zhang, Y.; Yang, W. Comment on "Generalized Gradient Approximation Made Simple". *Physical Review Letters* **1998**, *80*, 890.

[S15] Becke, A. D. Density-functional exchange-energy approximation with correct asymptotic behavior. *Physical Review A* **1988**, *38*, 3098.

[S16] Lee, C.; Yang, W.; Parr, R. G. Development of the Colle-Salvetti correlation-energy formula into a functional of the electron density. *Physical Review B* **1988**, *37*, 785.

[S17] Miehlich, B.; Savin, A.; Stoll, H.; Preuss, H. Results obtained with the correlation energy density functionals of Becke and Lee, Yang and Parr. *Chemical Physics Letters* **1989**, *157*, 200.

[S18] Perdew, J. P.; Wang, Y. Accurate and simple analytic representation of the electron-gas correlation energy. *Physical Review B* **1992**, *45*, 13244.

[S19] Wu, Z.; Cohen, R. E. More accurate generalized gradient approximation for solids. *Physical Review B* **2006**, *73*, 235116.

[S20] Kim, G.; Ma, K. Y.; Park, M.; Kim, M.; Jeon, J.; Song, J.; Barrios-Vargas, J. E.; Sato, Y.; Lin, Y.-C.; Suenaga, K.; Roche, S.; Yoo, S.; Sohn, B.-H.; Jeon, S.; Shin, H. S. Blue emission at atomically sharp 1D heterojunctions between graphene and h-BN. *Nature Communications* **2020**, *11*, 5359.

[S21] Tepliakov, N. V.; Lischner, J.; Kaxiras, E.; Mostofi, A. A.; Pizzochero, M. Unveiling and manipulating hidden symmetries in graphene nanoribbons. *Physical Review Letters* **2023**, *130*, 026401.